Sustinere
Journal of Environment and Sustainability
Volume 7 Number 1 (2023) 1-14

Print ISSN: 2549-1245 Online ISSN: 2549-1253
Website: https://sustinerejes.com E-mail: sustinere.jes@uinsaid.ac.id

**RESEARCH PAPER**

# Analysis of electrostatic precipitators plate-wire type in reducing dust emissions for sustainable environment

Herliati Rahman*, Cepy Hidayaturrahman
*Chemical Engineering, Faculty of Industrial Technology, Jayabaya University Jalan Raya Bogor km 28,8 Cimanggis Jakarta Timur, Indonesia*

Article history:
Received 16 November 2022 | Accepted 8 March 2022 | Available online 30 April 2023

**Abstract.** The current global environmental trend is that the world has agreed to go towards net zero emissions. Consequently, waste-producing-industries must comply with these provisions to achieve the mission of sustainable development and green production, including cement industry. This study aims to investigate the factors that affect the performance of the Electrostatic Precipitator (EP) as a dust collector in grinding cement raw materials. The method used was measuring the static-dynamic pressure at the poking hole closest to the EP inlet, measuring EP efficiency using the Matts-Ohnfeldt equation based on secondary data obtained from the Crane Information Management System (CIMS), and calculating the corona power to determine how strong the ion space is created between the discharge electrode and collecting electrode and determine the critical voltage and application voltage needed to generate the corona. The observations and calculations show that several factors can affect EP performance, such as inlet temperature gas discharge, concentration of dust from the chimney, and maximum concentration of chimney outlet. The maximum temperature gas discharge that EP can accept is 105°C. The maximum concentration of chimney outlet dust is 50 mg/Nm$^3$ and maximum CO concentration is 2000 mg/m$^3$.

**Keywords:** Efficiency; environmentally friendly; green concrete; net zero emission

## 1. Introduction

The cement industry can potentially cause environmental pollution in the form of dust particles and greenhouse gases such as Sox, NOx, and CO (Liew et al., 2017; Sivakrishna et al., 2020). Indonesia is rich in natural limestone resources, one of the primary raw materials for cement production (Rahman & Rahayu, 2021). Therefore, Indonesia is included as one of the world's cement-producing countries with many cement industries (Ningsih et al., 2019). In line with the mission of sustainable development and concern for environmental issues towards net zero waste (Abubakar et al., 2022; Habila, 2022; Obrist et al., 2021), the cement industry is required to meet the provisions of the opacity in every process that occurs (Panjaitan et al., 2020). The Indonesian government sets the highest particulate emission during the combustion process in the kiln at 80 mg/Nm$^3$. However, some companies even set a more stringent value of 55 mg/Nm$^3$ (Basel Convention Regional Centre for South East Asia, 2017; Gupta et al., 2012). In

*Corresponding author. E-mail: herliati@jayabaya.ac.id
DOI: https://doi.org/10.22515/sustinerejes.v7i1.295

general, each stage of the cement production process can generate particulate matter, such as the grinding stage of raw materials, the stage of clinker formation in the kiln, the stage of clinker transportation, and the final grinding stage (Devi et al., 2017).

The most significant potential for making particulate occurs in the kiln because of the confluence of air from the grate cooler with clinker coming from the kiln inlet hood (Ciobanu et al., 2021). Exhaust gas material containing cement dust flows to the top separator (SP) then divides into two streams towards the gas conditioning tower and tube mill, where it still contains particulate residue from combustion, called return dust (Nidheesh & Kumar, 2019). Exhaust gas containing dust first routed through the EP before being discharged through the chimney to avoid polluting the environment (Bataev et al., 2019). In addition to return dust, dust emissions are also generated from the excellent raw meal. The flue gas pushes fine particles, which then escape from the separator. These fine particles that escape is then trapped in the Electrostatic Precipitator (EP), which works based on electrostatic forces (Razlighi et al., 2019). Based on the design data, the minimum efficiency of EP Raw Mill can reach 99.95% (Sander & Fritsching, 2020). However, EP performance can decrease due to several factors, including EP inlet temperature, raw material fineness measurement, and organic compound content in raw material. Organic compounds can inhibit the ionization process of particles by corona plasma.

The purpose of this study is to analyze the performance of EP so that it can be identified what factors can cause a decrease in the performance of EP Raw Mills, thereby providing valuable information for management in making decisions on whether to replace the dust catcher in the Raw Mill. For EP efficiency calculations, the Matts-Ohnfeldt equation is used based on secondary data obtained from CIMS data. Then corona power calculations determine how strong ion space is created between the discharge and collecting electrodes. Moreover, knowing the critical voltage and application voltage needed to generate the corona.

## 2. Methodology

### 2.1. Sampling technique

The devices used during this study were pitot tubes and ABB's Crane Information Management System (CIMS). A pitot tube is a measuring tool used to determine the difference in static and dynamic pressure to determine gas flow and air volume entering through the EP inlet duct. A pitot tube is equipped with a pressure meter reading device HHP-2082 with a reading range of 0–200 kPa.

ABB's CIMS is an operational data processing center that can be read in real-time from the Central Control Room (CCR) based on Distribution Control System (DCS). The information collected includes process parameters in the Raw Mill area to the Finish Mill area. The parameters in question include weighing feeder tonnage, dust emission, EP inlet temperature, kiln parameter monitoring, vibration (Cano et al., 2017), and motor amperage. This study used CCR data from ABB's to obtain temperature and gauge pressure data at the measurement time and analyze the effect of secondary voltage (kV) and secondary current (mA) on EP performance and chimney emission. Measurements were taken twice between 08.00 - 10.00 a.m. on two different days.

### 2.2. Data collection technique

The pitot tube was inserted to two poking holes: the poking hole duct after the mill fan and the upper poking hole duct towards the EP inlet. This measurement determined the difference in the suction strength of the two ducts. More potent suction after the mill fan indicated static and dynamic pressure that was more negative or stronger than the pressure in the upper poking hole duct, which is closer to the EP inlet. An illustration of the measurement can be seen in Figure 1.

Static and dynamic pressure was recorded ten times with an interval of 10 seconds each. Static and dynamic pressure data were then processed to determine the gas flow rate (at 0°C and 1 atm pressure) and the gas discharge entering the EP inlet.

Only positive probes were used when measuring static pressure because the pitot tube was only needed to read the fluid flow hitting the tube's surface. Meanwhile, during dynamic measurements, both probes were used. The negative probe was connected to a tube in direct contact with the fluid flow. The positive probe was connected to one other tube.

Secondary data obtained from CIMS included EP inlet temperature data, secondary voltage, and current, which produced corona formation, opacity, and gauge pressure in each chamber which were read by CCR from instrumentation in the field in real-time. In order to obtain the migration speed, other secondary data was also needed, namely particle size distribution of EP dust obtained from the Quality Control (QC) Department, gas viscosity obtained from the interpolation of the flue gas calculation table based on the ratio of temperature and pressure assuming composition 13% $CO_2$, 11% water vapor $H_2O$, dan 76% $N_2$.

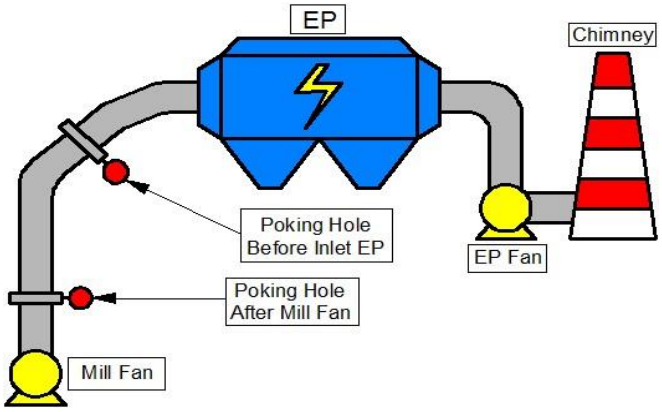


**Figure 1.** Illustration of measuring data on poking holes

## 2.3. Data processing and analysis technique

### 2.3.1 Data processing for calculation of gas volume and flow

The static and dynamic pressure data presented are the results of the average pressure measurement using a pitot tube with a coefficient of 0.85 (Usta et al., 2021). The duct used had a diameter (D) of 2.10 m and a cross-section area (A) of 3.46 $m^2$, while the thickness (width) and length (length) of the duct were ignored. With commonly used formulas, data on gas velocity, volumetric gas flow rate entering the EP, and gas flow with temperature conditions of 0°C and pressure of 1 atm were obtained.

### 2.3.2 Data processing for corona generation

The data required for the calculation are the radius of the electrode wire in units of m, relative gas density, experimental coefficients (A and B) representing the type of gas, and the polarity of the discharge, namely: A = 3.2×106 V/m; B = 9×104 $V/m^{1/2}$. In order to obtain the relative gas density value, data on the EP inlet temperature in Kelvin units and absolute pressure in kPa units are needed (Minkin et al., 2016). Absolute pressure can be obtained from the sum of the gauge pressure (the pressure read on CCR/CIMS) with 14.7 psi. By substituting the above data into Equation 1, the value of the electric field strength in the discharge electrode area was obtained before particles were present ($E_0$). The critical corona voltage or minimum voltage ($V_0$) needed to generate a corona was obtained from Equation 2 between $E_0$, the corona radius, and the distance between the wire and plate in m units. From the data $V_0$ and $E_0$, it can be calculated that the

application voltage was the voltage that could operate the EP. The last data obtained was the electric field strength after particles were present (Ep) based on Equation 3 between the application voltage ($V_0$) and the distance between the wire and plate in m units (Muzafarov et al., 2020).

$$E_o = A\delta + B\sqrt{\frac{\delta}{r_o}} \quad (1)$$

$$V_0 = E_0 r_0 ln\frac{R_0}{R_1} \quad (2)$$

$$E_P = \frac{V}{R_1} \quad (3)$$

### 2.4. Data processing to calculate migration speed and efficiency

Migration velocity (w) is obtained from Equation 4 between the gas viscosity in Pa.s, particle size distribution in units of m, and $E_0$ and Ep in units of V/m. The particle size distribution data were obtained from the QC Division. Moreover, the gas viscosity is obtained by interpolation from the Pipe Flow Calculation conversion table.

$$w = \frac{d_p E_0 E_p}{4\pi\mu} \quad (4)$$

The collecting plate area (A) was obtained from the specifications listed in the EP Baltic System Operation & Maintenance Manual of 15300 $m^2$. Gas discharge (Q) was obtained from the product of the area with the gas inlet velocity in units of $m^3$/second. The Matts-Ohnfeldt constant (k) was set at 0.5, considering that the standard deviation of the particle size distribution of EP dust is not more than 0.5. The above data was processed into the Matts-Ohnfeldt Equation to obtain the EP efficiency value (η) according to the actual conditions. In addition, EP efficiency calculations were performed (η) by comparing the inlet and outlet concentrations of EP, with the assumption that the inlet dust concentration (Di) was equal to 95000 mg/$Nm^3$ obtained from the initial specification data, and the outlet dust concentration (Do) was obtained from the opacity data in units mg/$Nm^3$. The Specific Collection Area is obtained by dividing the area of the collecting plate area and the volume of gas flow (Q) in m2 units (Razlighi et al., 2019). The Aspect Ratio is obtained from the equation's results between the number of chambers multiplied by the length of each chamber and then divided by the height of the chamber. The total dust captured can be calculated from the efficiency of EP (η) in decimal units multiplied by the volume of gas flow (Q) in units of m3/second, then multiplied by the density of raw meal, which is assumed to be 1.35 g/$m^3$.

## 3. Results and discussion

From the measurements made, primary data was obtained from static pressure and dynamic pressure from the EP inlet. These two pressures calculate the velocity, volume, and flow of gas entering the EP.

### 3.1. Gas flow and discharge calculation

To calculate the flow and discharge of gas inlet EP, the initial parameter needed was the gas density from the results of dynamic pressure measurements ($\rho_{dyn}$), obtained based on Formula 5. The results of static and dynamic pressure measurements in two different conditions are presented in Table 1.

$$\rho_{dyn} = 1.36\left(\frac{273}{273+T}\right)\left(\frac{10330+P_{dyn}}{10330}\right) \quad (5)$$

**Table 1.** Static and dynamic pressure measurement for two different conditions

| | | | | | | | | | | | |
|---|---|---|---|---|---|---|---|---|---|---|---|
| **Measurement 1 ($mmH_2O$)** | **Static** | -60 | -50 | -60 | -50 | -70 | -40 | -60 | -50 | -30 | -30 |
| | **Dynamic** | -40 | -30 | -20 | -10 | -30 | -20 | -30 | -30 | -20 | -30 |
| **Measurement 2 ($mmH_2O$)** | **Static** | -50 | -60 | -50 | -60 | -70 | -60 | -80 | -70 | -60 | -80 |
| | **Dynamic** | -20 | -20 | -40 | -30 | -40 | -30 | -30 | -20 | -20 | -30 |

In Measurement 1, with 10 observations, an average dynamic pressure of 26 mm $H_2O$ is obtained, so for an average temperature of 97.63°C, the calculation results of $p_{dyn}$ are 1 kg/m3 according to Equation 6. In contrast, in Measurement 2, with the same number of observations, in the same way, the result of $p_{dyn}$ calculation is 0.99 kg/m3, where the average dynamic pressure is 28 mmH2O with an average temperature of 99.51°C. Figures 2 and 3 show the static and dynamic pressure curves for two conditions.

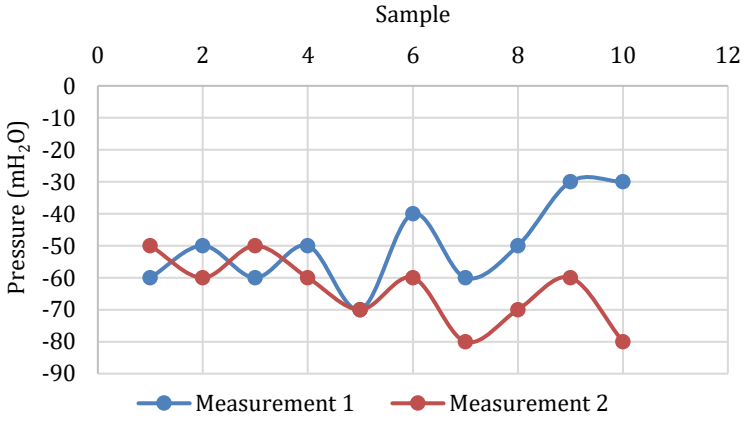


**Figure 2.** Static pressure curve

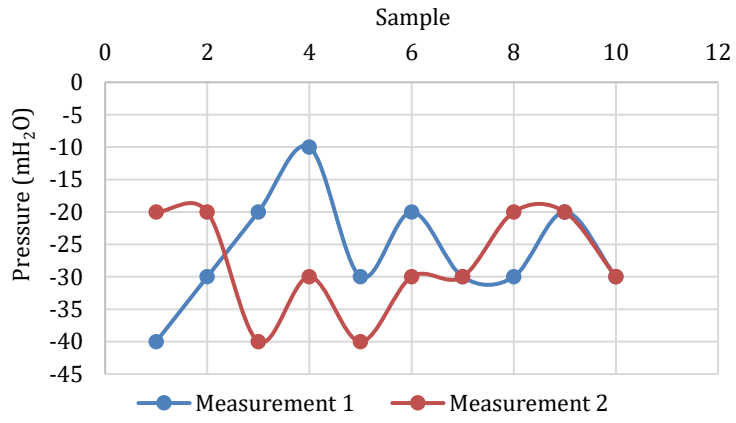


**Figure 3.** Dynamic pressure curve

It can be seen that the dynamic pressure curve is more volatile due to the turbulent flow of gas entering the negative pitot tube. After recording 10 times with a time lag of 10 seconds each, the static pressure in Measurement 1 is in the range of 30 to 70 mmH2O, while in Measurement 2, it is slightly higher, ranging from 50 to 80 mmH2O.

Dynamic pressure affects the gas velocity, while static pressure affects the discharge of flue gas entering the EP (Krupa et al., 2019). This is another variable that affects how much gas flows is the EP inlet temperature. The higher the temperature, the greater the inlet gas discharge. Initially, the temperature rise is caused by an increase in pressure which will make the duct space denser with air so that the temperature inside becomes hotter, as is the principle of a pressure vessel. Then the gas flow rate must be maintained by paying attention to the temperature indication because the optimum temperature that the maximum EP can accept is 105°C (Xu et al., 2016).

From the CIMS data, in Measurement 1, the average EP inlet temperature data = 97.63°C, Pstatic average 50 mm $H_2O$, and Pdynamic average = 26 mm $H_2O$. In Measurement 2, the data obtained was Pstatic = −64 mm $H_2O$, Pdynamic = −28 mm $H_2O$, and the inlet temperature was 99.51°C. Thus, it is proven that the value of static and dynamic pressure is directly proportional to the increase in EP inlet temperature and the quantity of flue gas flow.

Another parameter affecting the EP efficiency is the concentration of dust from the chimney (Li et al., 2019), which the CEM analyzer monitor. In Measurement 1, emission of 19.06 mg/$Nm^3$ was obtained, while in Measurement 2, it was 22.09 mg/$Nm^3$. The calculation results of efficiency (η), which involves a comparison between in and out concentrations, assuming that the concentration is constant, according to the specifications of 95000 mg/$Nm^3$, produces a η of 99.98% compared to the design specifications of 99.95%. The performance of the actual raw mill goes beyond the standards of Baltic Systems.

Formula 6 might then be used to calculate the gas velocity data (v), where k = 0.85 is the pitot tube coefficient. By substituting the ρdyn and Pdyn values into the above equation, the gas velocity at two different measurements can be calculated as 19.16 m/s and 19.94 m/s, respectively.

$$v = k\sqrt{2x9.81x\frac{(-P_{dyn})}{\rho_{dyn}}} \tag{6}$$

Meanwhile, the inlet gas volume (Q) is obtained from the product of the cross-section with the gas velocity and multiplied by 3600 to obtain units of cubic meters per hour. It is known that the duct diameter (D) = 2.10 m, ignoring the thickness (W) and length (L), then a cross-section area (A) of 3.46 $m^2$ was obtained. Therefore, the inlet gas volume in the two measurements are 238785.29 $m^3$/hour and 248451 $m^3$/hour, respectively. Moreover, the gas flow rate can be calculated using Formula 7 as follows:

$$Gas\ Flow\ Rate = Q\left(\frac{273}{273+T}\right)\left(\frac{10330+P_{stat}}{10330}\right) \tag{7}$$

Gas flow rates of 175036 $Nm^3$/h and 180955 $Nm^3$/h were therefore obtained in two different conditions.

### 3.2 Calculation of Corona Power

Corona power is needed to generate the corona (Gao et al., 2019). The first variable that must be known is the electric field strength before there are particles ($E_0$), the critical voltage or the minimum voltage needed to generate the corona ($V_0$), the application voltage (V), and the electric field strength after the particles are present ($E_p$).

In order to get the value of $E_0$, several parameters are needed, namely the radius of the discharge electrode ($r_o$), the relative density of the gas ($\delta$), and the experimental coefficients A and B. At first, the relative density of the gas is calculated by entering the gauge pressure, which is the pressure read by the measuring instrument from the CIMS. The gauge pressure is first converted to absolute pressure by adding 10332 $mmH_2O$. If it has been added up, it is converted to kPa units by multiplying by 0.01. At the same time, the temperature is converted into Kelvin. The average gauge pressure measurement in Observation 1 was −140.47 mmH2O. Thus, the absolute pressure of the EP inlet was 99.95 kPa, and in Observation 2 was 99.98 kPa.

Relative density is obtained from the empirical formula, which includes absolute pressure in kPa units and temperature in Kelvin units, as in equation 8. If the average temperature was 97.63°C, then the relative density of gas during Measurement 1 was 0.7955, while at an average temperature of 99.51°C in Measurement 2 is 0.7918.

$$\delta = 2.95\frac{P_{abs}}{T} \tag{8}$$

Another data to complete the calculation process was the electrode wire radius (DE) which was 0.003 m. Then it was known that the experimental coefficient A = $3.2\times10^6$ V/m and coefficient B = $9\times10^4$ $V/m^{1/2}$. So the magnitude of E0 can be determined by Equation 9 as follows:

$$E_0 = A\delta + B\sqrt{\frac{\delta}{r_0}} \tag{9}$$

After substituting all the values of A, δ, B, and r0, the E0 values are 4011.28 kV/m and 3995.95 kV/m.

After obtaining the electric field strength $E_0$, the following data to look for was the critical corona voltage, which is the minimum voltage needed to generate the corona field so that the dust can be captured by the electrostatic force optimally. The data needed to calculate the critical stress is the corona radius ($R_0$) and the distance between the wire and the plate ($R_1$). From the data $R_1$ of 0.20 m, $R_0$ could be obtained through Equation 10 as follows:

$$R_0 = R_1 + 0.02\sqrt{R_1} \tag{10}$$

If the $R_1$ value of 0.2 is substituted into equation 10 above, then the $R_2$ value of 0.21 m is obtained. While the critical stress value can be calculated by the following Equation 11:

$$V_0 = E_0 R_0 ln\frac{R_0}{R_1} \tag{11}$$

After all, values were substituted into Equation 11, and the critical voltage values are 36.67 kV and 36.53 kV.

The next step was calculating the application voltage ($V$) using Equation 12, namely the EP voltage so that it can operate. The applied voltage can be calculated from the data $V_0$ and $E_0$ at each measurement time. The application voltage for each measurement was 110.03 kV and 109.61 kV. Table 2 shows the results of calculating the field strength after the EP captured the particles.

$$V = V_0 + E_0\frac{R_0^2 - R_1^2}{R_1} \tag{12}$$

**Table 2**. Field strength after a particle is captured by the EP

| Parameters | V (kV) | $R_1$ (m) | $E_0$ (kV/m) | $E_p$ (kV/m) |
|---|---|---|---|---|
| Measurement 1 | 110.0291 | 0.2 | 4011.2834 | 550.1455 |
| Measurement 2 | 109.6085 | 0.2 | 3995.9494 | 548.0425 |

The amount of corona power can be obtained from the application voltage, critical voltage, and average corona current, namely the electrical power needed to generate the corona in each chamber, as shown in Tables 3 and 4.

**Table 3.** The corona power (Measurement 1)

| Chamber | $V_m$ (kV) | $V_p$ (kV) | $I_c$ (mA) | $P_c$ (kW) |
|---|---|---|---|---|
| #1 | 61.6 | 62.7 | 369.37 | 22.95635 |
| #2 | 6.4 | 67.0 | 146.20 | 5.36554 |
| #3 | 68.6 | 71.5 | 531.03 | 37.19865 |
| #4 | 31,8 | 36.0 | 733.37 | 24.86124 |
| | | | Total corona power, $P_c$ (kW) | 90.38178 |
| | | | Q ($m^3$/h) | 238785.29 |
| Total specific corona power, $P_c$/Q (watt per 1000 $m^3$/h) | | | | 378.506 |

**Table 4.** The corona power (Measurement 2)

| Chamber | $V_m$ (kV) | $V_p$ (kV) | $I_c$ (mA) | $P_c$ (kW) |
|---|---|---|---|---|
| #1 | 61.7 | 62.2 | 520.13 | 32.222054 |
| #2 | 62.5 | 63.9 | 255.03 | 16.117896 |
| #3 | 51.7 | 52.7 | 816.67 | 42.630174 |
| #4 | 28.9 | 28.9 | 1335.07 | 38.583523 |
| | | | *Total corona power,* $P_c$ (kW) | 129.553647 |
| | | | Q ($m^3$/h) | 248451 |
| *Total specific corona power,* $P_c$/Q (watt per 1000 $m^3$/h) | | | | 521.445 |

### 3.3 Calculation of migration speed

Migration speed is how fast the particles are loaded with electrons and then move to the collecting plate (Razlighi et al., 2019). Migration speed is influenced by particle size, electric field, and gas viscosity. The smaller the particle size, the harder it is to load electrons, so the migration speed is slower (Dong et al., 2018). However, if the electric field is more robust, the migration speed will be faster because the particles will be loaded with electrons faster from the discharge electrode.

The electric field strengths $E_0$ and Ep are known from the previous point. Meanwhile, the particle diameter is known from the particle size distribution, the results of two tests obtained from QC laboratory data, as can be seen in Figures 4 and 5.

According to the QC Department, EP dust samples were scooped up from the screw conveyor so that the particle size tested corresponds to the particle size entering the EP. Figure 4 above shows that the percentage of passing particle size distribution of EP dust is different in the two tests. This result indicates the fineness of the particles entering the EP inlet depending on the composition of the incoming material oxide and the operational conditions during the test (Long & Yao, 2010).

The average particle size of EP dust that passes 90% was 15-20 m. In addition, in the first measurement, EP dust particle size did not reach 100% passing through a 100 m sieve, only surviving on a 92.5% scale. This situation indicates that 7.5% of the particulates measuring more than 100 m enter the EP.

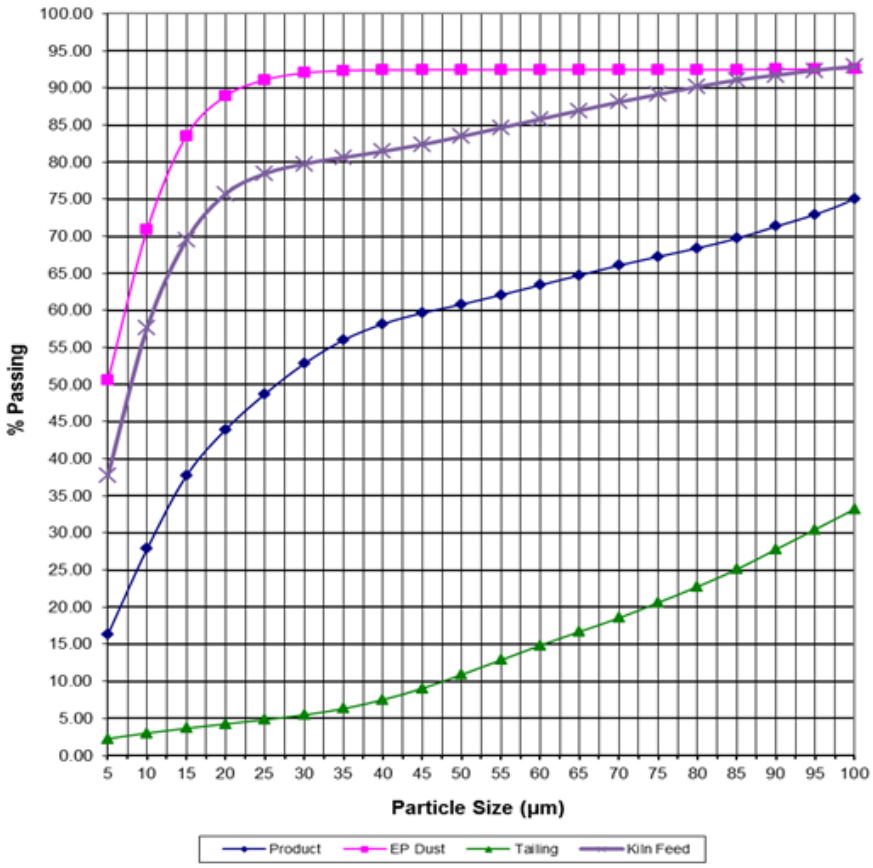


**Figure 4.** Particle size distribution curve (Observation 1)

Assuming that the maximum particle size that entered the EP was 130 m, and the minimum particle size refers to particles that pass 90% passing which is 15 µm, then the median value is determined to be 65. Therefore, the average particle size for calculating the next migration speed is 65 µm. In order to complete the parameters required for the calculation, finding the viscosity of the EP inlet gas is necessary. Gas viscosity is affected by temperature and pressure. The EP inlet pressure at Measurement 1 was 99,941 kPa; the viscosity value of this pressure was 21715246 Pa.s.

Particle size affects the speed of migration because microscopic particles have a small density, thereby reducing the rate of movement of particles toward the collecting plate (Gao et al., 2020). If so, the migration speed becomes slower, so the EP performance decreases. Table 5 displays the magnitude of the field strength at two different measurements.

**Table 5.** Electric field magnitude

| Parameters | $\mu$ | Particle size (DP) | | $E_0$ | Ep | w |
|---|---|---|---|---|---|---|
| | (Pa.s) | µm | m | V/m | V/m | m/s |
| Measurement 1 | 21715246 | 65 | 0.000065 | 4011076.42 | 550117.11 | 0.5259 |
| Measurement 2 | 21798342 | 65 | 0.000065 | 3995922.69 | 548038.78 | 0.5199 |

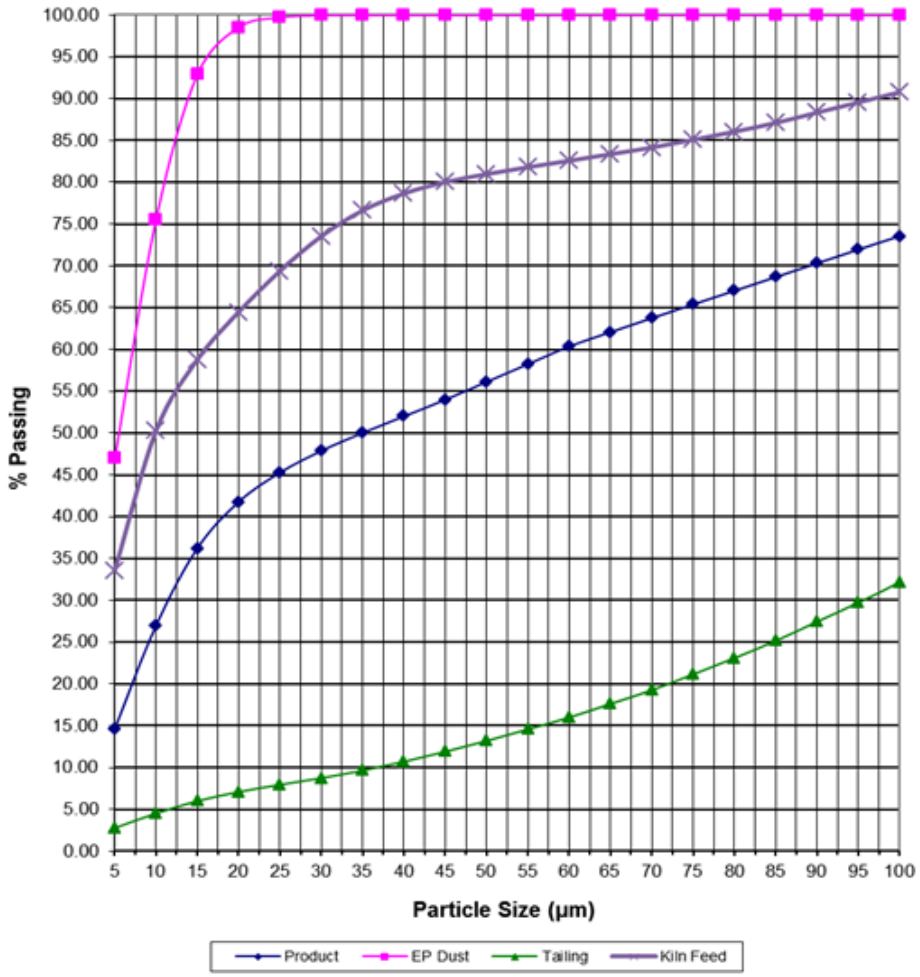


**Figure 5.** Particle size distribution curve (Observation 2)

### 3.6 Calculation of EP performance & efficiency

The calculation of EP performance and efficiency were obtained by Specific Collection Area (SCA), in-out concentration, and the Matts-Ohnfeldt Equation (Altun & Kilic, 2019). Table 6 shows the results of the SCA calculation on two observations. The performance calculation based on In-Out concentration can be calculated by Equation 13, where the inlet dust (Di) was 95000 mg/Nm$^3$, and the maximum concentration of chimney outlet dust was 50 mg/Nm$^3$. In order to obtain η of 99.95 %.

**Table 6**. Specific collection area

| Parameters | Q (m$^3$/h) | A (m$^2$) | *SCA* (m$^2$ per 1000 m$^3$/h) |
|---|---|---|---|
| Measurement 1 | 238785 | 15300 | 64.1 |
| Measurement 2 | 248451 | 15300 | 61.6 |
| Data Design | 600000 | 15300 | 25.5 |

$$\eta = \frac{D_i - D_0}{D_i} x100\% \quad (13)$$

Efficiency calculations based on the Matts-Ohnfeldt equation can be carried out with the assumption that the cross-section area (A) (Bäck Power Sweden AB, 2017) is 15300 $m^2$, the gas flow rate (Q) 238785.29 $m^3$/hour or 66.33 $m^3$/second. The k value is 0.5, and the average migration speed (wk) = 0.5259 m/s. By substituting all the values above into Equation 14, the efficiency value is 99.97%.

$$\eta = 1 - e^{-w_k\left(\frac{A}{Q}\right)^k} \quad (14)$$

From this efficiency value, it was possible to find the dust captured by EP and the dust that passed to the chimney, assuming a raw meal density of 1.35 g/$m^3$, 89.51 g/second.

### 3.6 Monitoring of emissions

Monitoring of gas emissions consisting of $SO_2$, NOx, and CO during the observation was stable, with a maximum CO concentration of 2000 mg/$m^3$ or 2% of the highest concentration of flue gas flow of 95000 mg/$Nm^3$. If the CO concentration has reached 2000 mg/$m^3$, the EP would automatically trip by the "CO Trip" interlock, whose high value was set at 2000 mg/$m^3$. This interlock was installed for safety reasons because a high CO concentration can potentially cause an explosion in the EP (Berhardt et al., 2017).

The CO concentration at the time of measurement was in the normal range between 0.1 – 1% of the total flue gas, with an average of 636.37 mg/m3 or 0.6699% of the total assumed volume of flue gas of 95000 mg/Nm3. The suitable concentration of CO (< 700 – 800 mg/m3) during the measurement period was due to the stability of the combustion process in the kiln, which used fuel with proper net calorific value, and the $O_2$ content in the EP was stable at 9 – 10%. The results of monitoring gas emissions during the study can be seen in Figure 6.

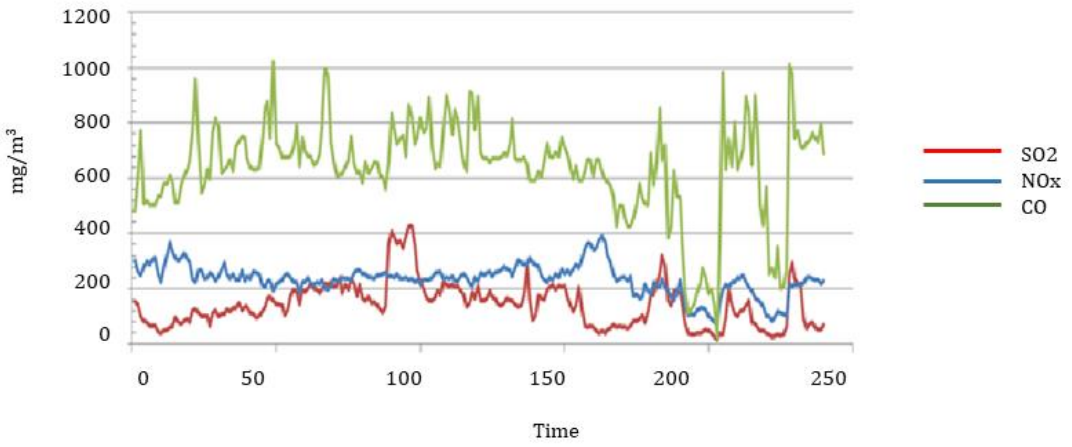


**Figure 6.** Greenhouse gas emission

### 3.6 Total organic carbon analysis

The appropriate parameter to evaluate the combustion process in the kiln is the Total Organic Carbon (TOC) value (Pirhadi et al., 2020). The organic carbon produced by burning in the kiln comes from alternative raw materials, alternative fuels, and the content of raw materials in the quarry. Suppose the quality of alternative fuels is not good. In that case, it will cause a large amount of organic carbon to circulate with secondary and tertiary air as return dust to Gas Conditioning Tower and tube mills.

**Table 7.** Carbon content in raw materials

| Sample name | *TC* (%) | *TIC* (%) | *TOC* (%) |
|---|---|---|---|
| *Limestone* | 9.9587 | 9.4204 | 0.5383 |
| *Clay* | 3.0708 | 0.9527 | 2.1181 |
| *Silica Sand* | 2.3348 | 0.6946 | 1.6402 |
| *Iron Sand* | 0.0733 | 0.0046 | 0.0687 |
| *EP Dust* | 10.1473 | 9.4499 | 0.6974 |
| *Material Stabilizer* | 9.9211 | 9.2154 | 0.7057 |

The TOC values for raw meal and cement kiln dust (return dust) influence clinker production. Raw meal as kiln feed is a source of TOC. Meanwhile, TOC contained in cement kiln dust indicates incomplete combustion, which can be affected by using primary fuels such as coal or alternative fuels (Bae & Kim, 2017).

Referring to the EN 13639 quality standard, the total TOC for limestone raw material is 0.2%. Table 7 shows the TOC value of limestone of 0.5383%. This condition indicates that there may be a decrease in EP performance. This result is in line with what has been reported in the literature that organic compounds can reduce the conductivity of the particulates in the EP and cause back corona events. As a result, the dust that enters the EP, both dust from the tube mill and returns dust carried from the combustion process in the kiln, will find it difficult to load electrons with the discharge electrode and then capture by the collecting plate due to poor conductivity.

Based on the results of interviews with the QC Department, the raw material from the old equipment (Quarry C) contains more organic compounds than the new equipment (Quarry A). This report can be the basis for management's consideration of replacing EP Raw Mill.

## 4. Conclusion

The results of observations and calculations that have been carried out on the performance and efficiency of EP Raw Mill conclude that several factors can affect the performance of EP. First, inlet temperature gas discharge; the maximum temperature that EP can accept is 105°C. The concentration of dust from the chimney also affects EP performance. The maximum concentration of chimney outlet dust is 50 mg/Nm3. Furthermore, it is necessary to maintain the CO concentration at a maximum of 2000 mg/$m^3$ or 2% of the maximum concentration of flue gas flow of 95000 mg/$Nm^3$. If the CO concentration is over 2000 mg/$m^3$, it can potentially cause an explosion in the EP.

## Acknowledgment

The author would like to thank PT Indocement Tunggal Prakasa Tbk. who have supported laboratory and library facilities.

## References

Abubakar, E., Shariff, R. Y., & Sadiq, Y. O. (2022). Deployment of treated and compressed biogas as a sustainable fuel for ceramic kiln firing. Sustinere Journal of Environment and Sustainability, 6, 14–25. https://doi.org/10.22515/sustinere.jes.v6i1.192

Altun, A. F., & Kilic, M. (2019). Utilization of electrostatic precipitators for healthy indoor environments. E3S Web of Conferences, 111. 02020. https://doi.org/10.1051/e3sconf/201911102020

Bäck Power Sweden AB, A. G. (2017). Relation between gas velocity profile and apparent migration velocity in electrostatic precipitators. International Journal of Plasma Environmental Science & Technology, 11(1), 104–111.

Bae, C., & Kim, J. (2017). Alternative fuels for internal combustion engines. Proceedings of the Combustion Institute, 36(3), 3389–3413. https://doi.org/10.1016/j.proci.2016.09.009

Basel Convention Regional Centre For South East Asia. (2017). Final Report Mercury Emissions From Coal-Fired Power Plants In Indonesia.

Bataev, D. K.-S., Salamanova, M. Sh., Murtazaev, S.-A. Yu., Viskhanov, S. S., & Murtazaev, S.-A. Yu. (2019). Utilization of cement kiln dust in production of alkali-activated clinker-free binders. Proceedings of the International Symposium “Engineering and earth sciences: Applied and fundamental research” Dedicated to the 85th Anniversary of H.I. Ibragimov (ISEES 2019). Atlantis press. 368-371. https://doi.org/10.2991/isees-19.2019.89

Berhardt, A., Lezsovits, F., & Groß, B. (2017). Integrated electrostatic precipitator for small-scaled biomass boilers. Chemical Engineering & Technology, 40(2). 278-288. https://doi.org/10.1002/ceat.201600200

Cano, M., Vega, F., Navarrete, B., Plumed, A., & Camino, J. A. (2017). Characterization of emissions of condensable particulate matter in clinker kilns using a dilution sampling system. Energy & Fuels, 31(8). 7831-7838. https://doi.org/10.1021/acs.energyfuels.7b00692

Ciobanu, C., Voicu, G., Istrate, I. A., & Tudor, P. (2021). Aspects regarding polluting emissions to the stack of clincher ovens in romanian cement factories. 42. 159-166. Advanced Engineering Forum, 42. https://doi.org/10.4028/www.scientific.net/AEF.42.159

Devi, K. S., Lakshmi, V. V., & Alakanandana, A. (2017). Impacts of cement industry on environment-an overview. 1. 156-161. Asia Pacific Journal of Research ISSN. www.apjor.com

Dong, M., Zhou, F., Zhang, Y., Shang, Y., & Li, S. (2018). Numerical study on fine-particle charging and transport behaviour in electrostatic precipitators. Powder Technology, 330, 210–218. https://doi.org/10.1016/j.powtec.2018.02.038

Gao, M., Zhu, Y., Yao, X., Shi, J., & Shangguan, W. (2019). Dust removal performance of two-stage electrostatic precipitators and its influencing factors. Powder Technology, 348, 13–23. https://doi.org/10.1016/j.powtec.2019.03.016

Gao, W., Wang, Y., Zhang, H., Guo, B., Zheng, C., Guo, J., Gao, X., & Yu, A. (2020). Numerical simulation of particle migration in electrostatic Precipitator with different electrode configurations. Powder Technology, 361, 238–247. https://doi.org/10.1016/j.powtec.2019.08.046

Gupta, R. K., Majumdar, D., Trivedi, J. V., & Bhanarkar, A. D. (2012). Particulate matter and elemental emissions from a cement kiln. Fuel Processing Technology, 104. 343-351. https://doi.org/10.1016/j.fuproc.2012.06.007

Habila, O. Y. (2022). Comparative analysis on perspectives of environmental and non-environmental NGOs on solid waste management in Jos metropolis, Nigeria. Sustinere Journal of Environment and Sustainability, 6, 26–43. https://doi.org/10.22515/sustinere.jes.v6i1.207

Krupa, A., Podliński, J., Mizeraczyk, J., & Jaworek, A. (2019). Velocity field of EHD flow during back corona discharge in electrostatic Precipitator. Powder Technology, 344, 475–486. https://doi.org/10.1016/j.powtec.2018.12.006

Li, S., Huang, Y., Zheng, Q., Deng, G., & Yan, K. (2019). A numerical model for predicting particle collection efficiency of electrostatic precipitators. Powder Technology, 347, 170–178. https://doi.org/10.1016/j.powtec.2019.02.040

Liew, K. M., Sojobi, A. O., & Zhang, L. W. (2017). Green concrete: Prospects and challenges. Construction and Building Materials, 156. 1063-1095. https://doi.org/10.1016/j.conbuildmat.2017.09.008

Long, Z., & Yao, Q. (2010). Evaluation of various particle charging models for simulating particle dynamics in electrostatic precipitators. Journal of Aerosol Science, 41(7), 702–718. https://doi.org/10.1016/j.jaerosci.2010.04.005

Minkin, M. S., Kuimov, D. N., & Lukyanov, A. D. (2016). Development of the Energy-saving Air Regeneration System in Production Rooms. Procedia Engineering, 150, 1353–1358. https://doi.org/10.1016/j.proeng.2016.07.327

Muzafarov, S., Tursunov, O., Balitskiy, V., Babayev, A., Batirova, L., & Kodirov, D. (2020). Improving the efficiency of electrrosatic precipitators. International Journal of Energy for a Clean Environment, 21(2). 125-144. https://doi.org/10.1615/InterJEnerCleanEnv.2020034379

Nidheesh, P. v., & Kumar, M. S. (2019). An overview of environmental sustainability in cement and steel production. In Journal of Cleaner Production. 231. 856–871. Elsevier Ltd. https://doi.org/10.1016/j.jclepro.2019.05.251

Ningsih, R. Y., Goembira, F., Komala, P. S., & Putra, N. P. (2019). Emission and heavy metal content characteristic of densified refused derived fuels of oil sludge and biomass combination as an alternative fuel for cement plant. Indonesian Journal of Environmental Management and Sustainability, 3(3), 100–105. https://doi.org/10.26554/ijems.2019.3.3.100-105

Obrist, M. D., Kannan, R., Schmidt, T. J., & Kober, T. (2021). Decarbonization pathways of the Swiss cement industry towards net zero emissions. Journal of Cleaner Production, 288. 125413. https://doi.org/10.1016/j.jclepro.2020.125413

Panjaitan, T. W. S., Dargusch, P., Wadley, D., & Aziz, A. A. (2020). Toward the best practice emissions reduction in an emerging economy: An analysis of cement manufacturing in indonesia. Entrepreneurship and Sustainability Issues, 8(1), 103–122. https://doi.org/10.9770/jesi.2020.8.1(7)

Pirhadi, M., Mousavi, A., & Sioutas, C. (2020). Evaluation of a high flow rate electrostatic precipitator (ESP) as a particulate matter (PM) collector for toxicity studies. Science of the Total Environment, 739. 104060. https://doi.org/10.1016/j.scitotenv.2020.140060

Rahman, H., & Rahayu, D. (2021). Characteristics of self compacting concrete (SCC) by the Silica Fume as portland cement substitute. Al-Kimia, 9(2), 115–123. https://doi.org/10.24252/al-kimiav9i2.21064

Razlighi, A. E., Asadi, M., & Nasrollahzadeh, B. (2019). Investigating migration velocity in the clinker cooler one stage electrostatic precipitator (made by ELEx, Hamon, and FLSmith Co.). Journal of Advances in Solid and Fluid Mechanics (ASFM). 1(1). 40-45.

Sander, S., & Fritsching, U. (2020). Dynamic flowsheet simulation of re-entrainment from particle layers formed inside electrostatic precipitators. Particuology, 53, 41–47. https://doi.org/10.1016/j.partic.2019.12.009

Sivakrishna, A., Adesina, A., Awoyera, P. O., & Kumar, K. R. (2020). Green concrete: A review of recent developments. Materials Today: Proceedings, 27, 54–58. https://doi.org/10.1016/j.matpr.2019.08.202

Usta, M. C., Uibu, M., Yörük, C. R., Tamm, K., Kuusik, R., Trikkel, A., Gastaldi, D., & Canonico, F. (2021). Mineral sequestration of CO2 from Vernasca Ca-looping demo system: scale up to a pilot. Proceedings of the 15th Greenhouse Gas Control Technologies Conference 15-18 March 2021, SSRN Electronic Journal. https://doi.org/10.2139/ssrn.3812245

Xu, X., Zheng, C., Yan, P., Zhu, W., Wang, Y., Gao, X., Luo, Z., Ni, M., & Cen, K. (2016). Effect of electrode configuration on particle collection in a high-temperature electrostatic precipitator. Separation and Purification Technology, 166, 157–163. https://doi.org/10.1016/j.seppur.2016.04.039